Environmental Science Nano

The role of secondary metabolites in the production of CuO nanoparticles by fungi: A physiological and metabolic approach

Journal:	*Environmental Science: Nano*
Manuscript ID	EN-ART-05-2024-000403.R1
Article Type:	Paper

Statement of significance

Fungi are known to produce nanoparticles, and previous research suggested this synthesis is linked to the secretion of certain biomolecules. However, little is known about the specific conditions that trigger this process or the chain of reactions for this synthesis. In this study, we investigated a fungus commonly found in the environment, *i.e. Penicillium pimiteouiense,* to investigate the production of copper oxide nanoparticles. We found that the synthesis of these nanoparticles occurs as secondary metabolites that are secreted into the growth media. Factors such as temperature, pH, and growth phase also affect the production of these metabolites. We also identified specific biomolecules involved in the synthesis of the nanoparticles, including NADPH-dependent reductases and secondary metabolites with phenolic groups. Oxidases were also found to play a role in the process. This study sheds new light on the process of nanoparticle synthesis by fungi.

ARTICLE

Received 00th January 20xx,

Accepted 00th January 20xx

DOI: 10.1039/x0xx00000x

The role of secondary metabolites in the production of CuO nanoparticles by fungi: A physiological and metabolic approach

Ying Zhou[a, b], Hang N. Nguyen[b], Janire Peña-Bahamonde[b], Francisco C. Robles-Hernandez[c,d], Luciana Jandelli Gimenes[e], Debora F. Rodrigues[b,d*]

Previous studies showed that the biosynthesis of nanoparticles by diverse fungi is linked to the secretion of NADPH/NADH in the growth media. The results of these studies suggested that the mechanism of synthesis of nanoparticles is a generic pathway used by diverse fungi to synthesize different nanoparticles. However, very few studies have performed a systematic investigation to understand the conditions triggering the secretion of these essential biomolecules for the synthesis of nanoparticles or the chain of reactions leading to the production of biosynthetic nanoparticles by fungi. In the present study, we isolated the fungus *Penicillium pimiteouiense* from a copper mine in Brazil. Species of this genus have been previously described to synthesize different nanoparticles. In the present study, we determined that this fungus can secrete metabolites for the rapid (within 10 min) biosynthesis of copper oxide nanoparticles (CuO NPs) with a size range between 50 and 60 nm. The production of these secondary metabolites is mainly affected by temperature, pH, type of growth media, and growth phase, but not by the presence of Cu^{2+}. Metabolomics was used to further elucidate the chain of reactions in the synthesis of CuO NPs. According to the results, NADPH (Nicotinamide adenine dinucleotide phosphate) dependent reductases (with NADPH as a cofactor), and secondary metabolites with phenolic groups were involved in the pathway as bio-reductants converting Cu^{2+} to CuO. The CuO NPs were further stabilized with peptides and other biomolecules, which served as capping agents leading to the thermodynamic stability of CuO NPs with a defined shape and size. This study confirms the previously reported role of NADPH/NADH in the synthesis of nanoparticles but brings additional information concerning other important biomolecules from fungal metabolites that also play a role in the biosynthesis of nanoparticles. Furthermore, this study identifies important physiological growth conditions that can affect the production of such metabolites. This work provides a deeper mechanistic insight and potential commercial opportunities for recycling metal-rich mine wastes and green fabrication of nanoparticles.

Introduction

Over the past decade, engineered metallic nanomaterials have been of great interest to the scientific community due to their various applications in nanotechnology. Copper oxide nanoparticles (CuO NP) typically exhibit a monoclinic structure with a direct band gap ranging from 1.6 to 3.2 eV, which is an attractive p-type metallic oxide semiconductor and widely considered an excellent electrode material.[1] This nanomaterial also has unique optical, electrical, and catalytic characteristics.[2-4] Additionally, the surface plasmon resonance (SPR) of CuO NP is remarkable and therefore has been widely used in photonic and photo-electric applications.[5-7]

According to global projections, the annual production of Cu-based nanoparticles will reach 1,600 tons by the year 2025.[8] CuO NPs are commonly synthesized using various methods including chemical reduction,[9] electrochemical,[10] thermal reduction,[11] solid state reaction,[12] sol-gel processing,[13] and hydrothermal methods.[14] Therefore, the current synthesis of CuO NPs requires laborious processes including the use of toxic chemicals.[15] Due to the increasing demand for this type of nanomaterial, recent studies have shifted efforts to investigate clean, eco-friendly, low energy intensive, and low-cost 'green' synthetic routes. In this context, the use of microbes[16] (such as bacteria, algae, and fungi) for producing bio-reductants for the synthesis of nanoparticles has attracted attention. Among all microorganisms, fungi are promising since they have a unique physiology, which involves secreting several extracellular enzymes, proteins, and small molecules to degrade and synthesize new compounds as well as stable nanoparticles.[17-19] Hence, nanoparticles synthesized by fungi can be a sustainable alternative to toxic chemical synthesis methods. Also, Fungi have been regarded as "nanofactories" since large volumes of nanoparticles can be produced by increasing the fungal growth medium volume for easy scale-up.

[a] Department of Materials Chemistry, Huzhou College, Huzhou 313000, P. R. China
[b] Department of Civil and Environmental Engineering, University of Houston, Houston, TX 77204-4003, U.S.A.
[c] Department of Mechanical Engineering Technology, University of Houston, Houston, TX 77204-4020, U.S.A.
[d] Department of Material Science and Engineering, University of Houston, Houston, TX 77204-4003, U.S.A.
[e] Center for Environmental Research and Training, University of São Paulo, Cubatão, São Paulo 11540-990, Brazil
*Corresponding authors: dfrigirodrigues@uh.edu, phone: +1-713-743-1495

† Footnotes relating to the title and/or authors should appear here.
Electronic Supplementary Information (ESI) available: [details of any supplementary information available should be included here]. See DOI: 10.1039/x0xx00000x

Earlier studies have demonstrated that proteins and/or other biomolecules can control the nucleation and growth of nanostructures and subsequently stabilize the nanoparticles.[20, 21] Some studies have hypothesized that the biosynthesis mechanism of metallic nanoparticles involved oxidoreductases, other cofactors (such as NADPH reductase), and secondary metabolites.[22] However, there is still very limited information available on the specific types of secondary metabolites, enzymes, and enzymatic reactions involved in this biosynthetic process. Other studies suggested that specific growth conditions are necessary to achieve the synthesis of nanoparticles by microorganisms.[23] However, no comprehensive and systematic study has been previously done to connect and elucidate the environmental conditions affecting nanoparticle synthesis and the actual synthetic mechanism of CuO NPs. So far, there is only fragmented information about the synthesis mechanisms. This study aims to obtain a holistic view of the biosynthesis of nanoparticles, using CuO NPs and an environmental isolated fungus as model systems.

In this study, we use *Penicillium pimiteouiense* as a model organism to produce CuO NPs. *Penicillium* sp. belongs to a genus known to be involved in the production of diverse nanoparticles.[24] This microbial strain was isolated from a soil sample collected in a copper mine. This study's primary aim was to perform a systematic investigation with *P. pimiteouiense* to determine the growth parameters and metabolites needed to produce CuO NPs. The overall objectives of this research included: i) to identify optimum conditions for fungal growth and for CuO NPs synthesis, ii) to characterize and determine the nanostructure of the biosynthetic CuO NPs under the optimum conditions, and iii) to disclose the specific biosynthetic pathway of CuO NPs based on unique metabolites and enzymes secreted by the fungus.

Materials and methods

Reagents

The chemicals purchased from Sigma Aldrich included malt extract, yeast extract, D-glucose, peptone, potato dextrose broth (PDB), NADPH (≥ 97 % (HPLC grade)), potassium phosphate (≥ 98 %), sodium sulfite (97 %), acetone (> 99.5 %), commercial CuO NPs (< 50 nm). The other chemicals were purchased from other companies: potato dextrose agar (PDA, dehydrated, BD Difco™), $CuSO_4.5H_2O$ (98 %, Spectrum Chemical Mfg. Corp.), and ethanol (absolute anhydrous, PHARMCO-AAPER).

Identification of *P. pimiteouiense*

P. pimiteouiense was collected and isolated from a soil sample in the Sossego Copper Mine (Pará State, Brazil, latitude 06°26'S and longitude 50°4'W). Single fungal colonies were isolated on Potato-Dextrose-Agar (PDA) by serial dilution. The screened strain was incubated and further purified at 28 ℃ for 7-10 days. The identification of the isolate was performed according to morphologic and molecular methods. Morphologic methods were based on the observation of microscopic and macroscopic structures, and specific identification keys.[24] The micromorphology of *Penicillium* spp. was determined by the presence of phialides, conidiophores, and septate hyphae. The morphologic characteristic of *Penicillium spp.* (Figure S1) was consistent with the fungal-specific taxonomic identification key and related literature for this genus.[24] For the molecular method, the identification of the fungus was based on Internal transcribed spacer (ITS) sequencing to determine the phylogenetic relationship of the isolate with other closely related *Penicillium* species.[25] The primers used for amplification and sequencing were ITS1 and ITS 4 (Internal transcribed spacer, ITS).[26, 27] Contig assembly and editing were done with Sequencer DNA Sequence Assembly Software 4.1.4 (Gene Codes Corporation, USA). The obtained sequence was compared using the BLAST algorithm with closely related sequences within the Sequencher DNA Sequence Assembly Software 4.1.4 (Gene Codes Corporation, USA). BLAST analysis showed that the isolate had a similar sequence to *P. pimiteouiense* species according to the NCBI genomic[28] and MycoBank databases.[29] The sequence of the isolate was deposited in the NCBI database with the following accession number: MK956944. The confirmed morphological characteristics and the ITS sequence allowed the identification of the fungus as *P. pimiteouiense*.

Optimization of copper oxide nanoparticles synthesis by *P. pimiteouiense*

P. pimiteouiense was initially plated on potato dextrose agar (PDA) (at pH 7.0 ± 0.3) for 10 days to reach a stable, mature growth. Then, three plugs of the fungus were transferred with a sterile 100 µl pipette tip to three sterile 250 mL Erlenmeyer flasks containing 100 mL of sterile malt-yeast-glucose-peptone (MYGP) medium (10 g/L glucose, 3 g/L malt extract, 1 g/L yeast extract, 5 g/L peptone, pH 7.0) supplemented with 150 mg/L chloramphenicol. The cultures were grown for 10 days. To determine the exact fungal mycelium dosage (~0.36 g), the mycelium was collected from each flask via filtration with a sterile paper filter (Whatman™ number 1) followed by 0.22 µm PVDF (Polyvinylidene difluoride) membrane filtration (Dow Corning), after that, the biomass was dried at 60 ℃ until constant weight was obtained. The cell-free supernatant from each flask was also collected to determine the secreted proteins/enzymes and metabolites by the fungus in the MYGP medium. All experiments were performed in triplicate. To initiate the synthesis reaction, copper sulphate stock solution (0.1 M copper ion) was mixed with 100 mL of the filtered supernatant to reach a final concentration of 5 mM Cu^{2+} and then further incubated for 6 h at room temperature. The

biosynthesis of CuO NPs was monitored by regular sampling to observe changes in the absorbance between the wavelengths 300 nm and 700 nm (UV–vis spectrophotometry, Synergy MX Microplate reader, BioTek, USA) as well as any colour changes in the medium. The control samples were prepared and incubated in parallel with the samples. The controls were sterile MYGP media at pH 7 with or without 5 mM copper ions.

Potato dextrose broth (PDB) medium and malt-glucose-peptone (MGP) were also tested as described above to determine the best growth media for nanoparticle production. After that, to achieve the best yield of CuO NPs, other different environmental and growth parameters were also investigated, including the fungus growth phase on the plate before transferring to liquid media (3, 5, 7, 10, 12, 15 days), the pH of the media (4.0, 7.0 and 10.0 ± 0.2), copper concentrations in the supernatant of the liquid media (1, 5, 10 and 20 mM Cu^{2+}), the growth temperature (8 ℃, 18 ℃, 28 ℃), and CuO NPs synthesis time (10 min, 1 h, 2 h, 3 h, 4 h, 5 h, 6 h, 18 h, 24 h and 48 h). Each environmental condition was investigated by altering one parameter at a time while keeping the other parameters constant. The synthesis of CuO NPs in each environmental condition was determined via UV-vis adsorption, as described earlier, and the results were normalized to the fungal biomass. The experiments were performed in triplicate for each parameter and the standard deviations were calculated.

Measurement of NADPH-sulphite reductase activity

NADPH-sulphite reductase activity was measured based on the self-oxidation of NADPH without sulphite.[8, 30, 31] In brief, NADPH-sulphite reductase was determined with the cells grown in three different media, namely: MYGP, MGP, and PDB, at 18 ℃ for 6 h. After growth, the cell-free supernatants were collected by filtration with sterile 0.22 µm filter membranes. Then, aliquots of 1 ml of the supernatants were transferred to 15 ml test tubes that contained 5 ml of 0.5 mM sodium bisulphite (Sigma Aldrich, 97 %), 1 ml of 0.02 mM NADPH, and 5 ml of 0.5 M potassium phosphate buffer (include 0.1 mM Na_2EDTA, pH 7.7). After that, the NADPH-dependent redox reaction was done by incubating the mixture under 100 rpm (revolution per minute) at 25 ℃ for 60 min. The control samples were prepared in parallel by replacing sodium sulphite with DI water to determine the oxidation of NADPH in the absence of sulphite. The experiments were performed in triplicate for each test and the standard deviations were calculated. One unit of activity was defined as that amount of enzyme catalyzing the sulphite-dependent oxidation of 1 nmol of NADPH per hour under the above conditions.[8, 31] The results were expressed in terms of change of NADPH, which was calculated from Equation (1).

$$\text{Enzyme activity}(U) = \frac{N \cdot M}{T} \cdot (\%\Delta A) - C \quad (1)$$

Where: N is the dilution of the samples; M is the volume of the supernatant sample (1 mL); T is the reaction time (1 h); C is the decreased amount of NADPH due to the oxidation (nmol), which can be obtained from the NADPH standard curve (plotted as the absorbance against NADPH concentration) based on the decrease in absorbance (A_{340}, Synergy MX Microplate reader, BioTek, USA) of the tested samples.

Characterization of copper nanoparticles produced under optimized conditions

The characterization of the nanoparticles was done with CuO NPs produced under optimum growth conditions, which involved growing the fungus in the MYGP medium at 18 ℃ for 10 days followed by the addition of 5 mM copper ions (from copper sulphate) to the medium supernatant for 6 h. The produced particles were collected via filtration with a paper filter (Whatman™ number 1) followed by 0.22 µm syringe filter membrane filtration, washed by 15 min with acetone first then ethanol and water for five cycles to remove any other cellular materials and impurities. After that, the filtrated samples were freeze-dried and washed with acetone and ethanol respectively to remove any other cellular materials and impurities. The purified CuO NP samples were freeze-dried for characterization. The transmission electron microscopy (TEM) was done on dry powders, the CuO powders were suspended in ethanol and an aliquot (5-10 µl) was transferred to a 200 mesh Cu grid. The grid was allowed to dry, and the TEM observations were made. The high-resolution transmission electron microscopy (HRTEM) was conducted on a JEOL JEM2000FXII. The images were analysed using Digital Micrograph and the d-spacing was supported based on the CIF-file (mp-704645) and Vesta® software. The Raman characterization was done on a confocal micro-Raman microscope XploRATM, Horiba JY. A 638 nm diode laser was used for excitation. The X-ray photoelectron spectroscopy (XPS) measurement was conducted using PHI 5700. The detailed XPS operation procedure was described in our previous study (refer to supporting information).[32] Fourier Transform Infrared Spectroscopy Nicolet iS10, equipped with Nicolet Smart ATR (FTIR), was used to assess the secondary structure of the biosynthesized CuO NPs. X-ray diffraction (XRD) was carried out using RIGAKU Miniflex 600. The aqueous CuO nanoparticle suspension (2 mg/L, pH 7.0) was dispersed in 10 mM $NaNO_3$ solution for zeta potential analysis (DLS, Zeta sizer Nano, Malvern Industry Ltd). Each measurement was done five times with 12 runs in triplicate at 25 ℃, and an equilibration time of 30 s.

Analysis of non-targeted extracellular metabolomics using LC-MS/MS

The fungal mycelium was incubated for 6 h in two different media (MYGP and PDB) under the optimized conditions (pH=7, T=18 ℃). Then, the supernatants were harvested immediately

at the end of the cultivation by filtration with a sterile paper filter (Whatman™ number 1) followed by another filtration with 0.22 µm PVDF membrane (Dow Corning). The corresponding MYGP and PDB media without fungi were also prepared in parallel as negative controls, respectively. Then, the prefiltered samples were stored at -20 ℃ before LC-MS/MS analysis.

An aliquot of 2 µl of the above samples and controls, which contained or did not contain the extracellular metabolites of the fungus, was analysed using Thermo Scientific™ Q Exactive™ LC-MS/MS system (Thermo Fisher Scientific, San Jose, CA, USA). The extracellular metabolomics was separated through a Thermo Scientific™ Hypersil GOLD™ C18 UHPLC (Ultra-High-Performance Liquid Chromatography) reverse phase column (150 × 2.1 mm, 1.9 µm particle size). The LC mobile phases included 0.1 % formic acid in methanol (v/v) and 0.1 % formic acid in H_2O (v/v), respectively. The separation was performed with 99 % mobile phase A at a flow rate of 450 µL/min and temperature of 55 ℃ with an injection volume of 5 µL. The MS analysis was done on a Thermo Scientific TM Q Exactive TM mass spectrometer fitted with electrospray ionization (ESI). Top 4 MS/MS (ddMS2) spectra and high-resolution full-scan MS were obtained at a resolving power of 17,500 and 70,000 (FWHM m/z 70 to 1050). Sample analyses were conducted in both positive and negative electrospray ionization (ESI) modes as separate LC-MS/MS runs.

In this experiment, the Compound Discoverer™ software (2.1 SP1version, Thermo Scientific) was used for database search, differential analysis (including volcano plot), and KEGG pathway (Kyoto Encyclopedia of Genes and Genomes) analyses based on MS and mz Cloud fragmentation library. Using this software, the media components were first subtracted from the metabolites produced during growth on both MYGP and PDB media. For the background subtraction, all compounds present in the control media with higher (or comparable) levels than the testing supernatant samples were removed from the analysis. For the final analysis of the metabolites, only the interested compounds secreted by the fungus in MYGP medium (with CuO NPs production) and not in PDB (without CuO NPs production) were further analysed for identification of the CuO NPs synthesis pathway.

Results and discussions

Environmental and growth conditions affecting nanoparticle biosynthesis

We first determined the ability of the fungus to grow and produce CuO nanoparticles (NPs) under different growth and environmental conditions. First, the fungus was exposed to different growth media. The media investigated were malt–yeast–glucose–peptone (MYGP), malt–glucose–peptone (MGP), and potato dextrose broth (PDB). Subsequently, we evaluated the effects of pH and temperature on the fungus growth and copper salt concentrations to produce NPs. This physiological investigation allowed the identification of the optimum growth conditions triggering the production of metabolites containing reductases and biomolecules involved in CuO NPs production.

The production of CuO NPs was initially monitored using UV-Vis and visual inspection. In the case of visual inspection, we observed that as the fungal growth medium supernatant was exposed to copper sulphate, the colour of the medium changed from brown yellow to chartreuse whenever CuO NPs were produced (Figure S2a). This change in colour of the supernatant with the addition of copper sulphate was only observed when the fungus was grown in the MYGP medium (not in PDB and MGP medium). No colour change was observed for media control and supernatant control samples (Figure S2) in all three media.

In the case of the UV-Vis method, previous studies have described a sharp surface plasmon resonance (SPR) peak centering at 330 nm in the presence of CuO NPs.[33] The presence of this peak at 330 nm suggests the presence of small-sized, monodispersed CuO NPs according to the Mie theory.[34, 35] In this study, the MYGP medium exhibited the characteristic CuO NPs peak at 330 nm (Figure 1a). In contrast, in the PDB and MGP media, the characteristic peak was absent.

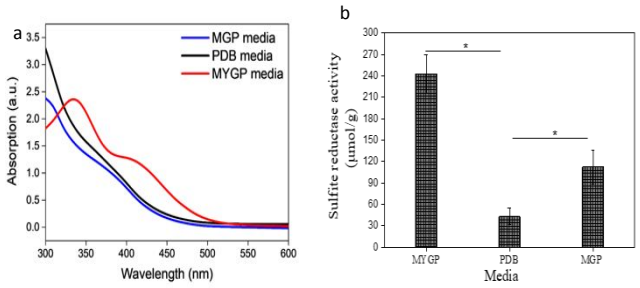

Figure 1. Effects of different growth media on the production of CuO NPs and secretion of NADPH-sulphite reductase. (a) The UV-vis spectra of the supernatant of MYGP, PDB, and MGP exposed to 5 mM of Cu^{2+}. The results show the synthesis of CuO NPs with MYGP media only, which correlated well with the reductase results. **(b)** Normalized NADPH-sulphite reductase refers to the determined NADPH-sulphite reductase divided by the dried mycelium (g) based on the enzymic activity calculation from Equation (1). The results showed higher NADPH-sulphite reductase production in the supernatant from the fungus grown in MYGP than PBD or MGP. Error bars indicate the standard deviation of the triplicate experiments. *P<0.05 significant difference.

In addition to investigating the ability of the fungus to produce CuO NPs on different media, we also evaluated the

production of candidate enzymes involved in CuO NPs synthesis (Figure 1b). Previous studies have suggested that NADPH sulphite reductase could participate in the reduction of metal ions to form Cu/CuO NPs.[36-38] In this study, the spent supernatant (*i.e.* media collected after microbial growth) was collected to determine whether NADPH-dependent sulfite was secreted by the fungus. The NADPH sulfite reductase activity in MYGP media was six- and two-fold higher than in PDB and MGP media, respectively (Figure 1b). The results suggest that the MYGP medium triggered the production of NADPH sulphite reductase by *P. pimiteouiense*, which could be playing a role in promoting the formation of CuO NPs.

The formation of nanoparticles can be influenced by varying concentrations of enzymes, proteins, and metabolites, contingent upon their respective growth phases and environmental conditions.[39,40] Figure 2 shows the results of UV–Vis absorbance at 330 nm of the CuO NPs synthesized and normalized by the fungal dry biomass from 3 to 15-day-old fungal cultures in MYGP. We observed that 3, 5, 7- and 10-day-old cultures exhibited a steady increase in the SPR peak and reached a maximum SPR peak on day 10, which corresponded to the late exponential growth phase of the fungi. After 10 days, we observed a decrease in the SPR peak intensity, which corresponded to the stationary phase. In the 15-day-old fungal cultures, no CuO NPs were synthesized. Therefore, the optimal production of CuO NPs was observed in the late exponential growth phase. In that growth phase, fungi secrete the maximum amount of secondary metabolites, which indicates the possible involvement of secondary metabolites in the synthesis of CuO NPs.[41] This hypothesis was further investigated later in this study.

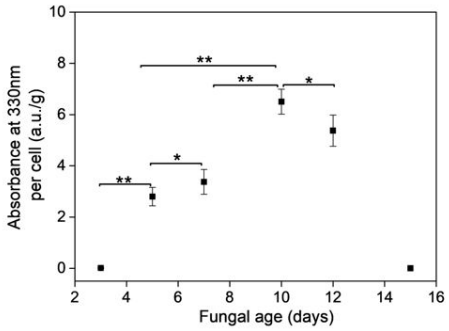

Figure 2. Effects of culture age on CuO NPs synthesis. Error bars indicate the standard deviation of triplicate experiments. The absorbance at 330 nm was normalized by the dried biomass. * $P < 0.05$, ** $P<0.005$ indicate statistically significant difference. The UV-vis absorbance curves are presented in the supporting information (Figure S3).

In addition to the enzymatic activity analysed, the incubation conditions, such as copper ion concentrations, pH, temperature, and nanoparticle production rate, were also investigated to determine the optimal conditions to produce secreted enzymes from *P. pimiteouiense* for CuO NPs synthesis (Figure 3). For the effect of the different environmental parameters, the MYGP medium was used. To evaluate the influence of the different dosages of Cu^{2+}, different concentrations of Cu^{2+} (1, 5, 10, 20 mM) were investigated (Figure 3a). The dosage of 5 mM Cu^{2+} was found to be optimal, which is aligned with the typically reported metal dosing range for other fungi (1~10 mM).[42, 43] When the initial copper ion concentration was 1 mM and 20 mM, the SPR peak was not present (Figure 3a). With 5 mM Cu^{2+}, the SPR peak was significantly higher than the peak obtained with 10 mM Cu^{2+}, especially at 18 °C and pH 7, which suggested that the maximum productivity of CuO NPs was with 5 mM Cu^{2+}. The concentration dependency in Cu ions during biosynthesis is probably related to the saturation of the enzyme with the substrate. The amount of enzymes or metabolites might not be enough to reduce metallic ions and cap the nanoparticles at higher metal dosages, which is likely due to the increased metal toxicity.[44]

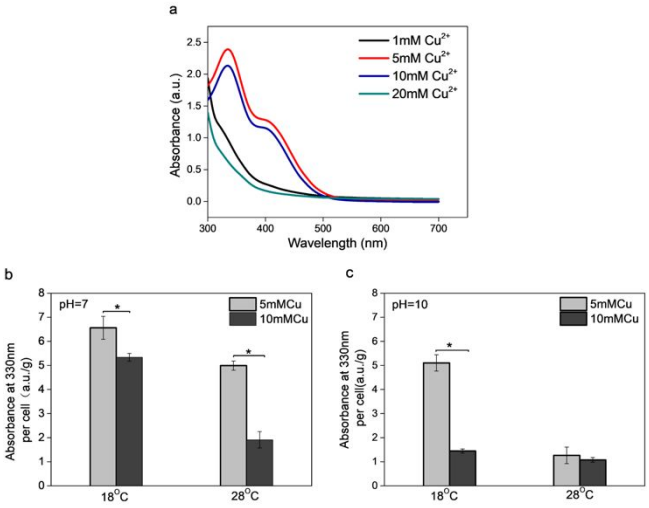

Figure 3. Effects of different copper sulfate concentrations, pH, and incubation temperature on CuO NPs synthesis. The UV-vis adsorption peaks of the supernatant of MYGP culture were measured under different conditions. (a) Effects of copper concentrations on CuO NP synthesis @ pH=7 and T= 18 °C. The concentration of 1 mM Cu^{2+} and 20 mM Cu^{2+} did not show any peaks, which suggests that no CuO NPs were produced as compared to 5 mM and 10 mM Cu^{2+}. (b) and (c) are the absorbance normalized by fungal dried biomass showing the effects of temperature and pH on CuO NPs production, respectively. * Indicate statistically significant difference with $P< 0.05$. The absorbance peaks were not observed @pH=4 and T= 8 °C. The detailed UV-vis absorbance curves are presented in the supporting information (Figure S4).

To study the effects of pH and temperature on the synthesis of CuO NPs, the pH of MYGP broth was adjusted to 4, 7, and 10 for fungal growth (please see supplemental information with additional results). The fungus cultured at these three pH values were incubated at 8 °C, 18 °C, and 28 °C to obtain supernatants

for the synthesis of CuO NPs. The supernatants were then exposed to 5 mM and 10 mM Cu^{2+}. Figures 3b and 3c present the results obtained at pH 7 and 10, respectively, at 18 °C and 28 °C, at which NPs were produced. The other conditions are not presented since they did not produce nanoparticles, additional data is presented in the supporting information (Figure S4). It is possible that at the conditions where there was no production of CuO NPs, there was a decrease in the production of capping agents. [45] Furthermore, the results obtained upon varying pH of the medium agree with previous studies that the maximum production of metal NPs using fungi occurs in a neutral environment.[46] The optimal incubation temperature was found to be 18 °C, at which the yield of CuO NPs was higher than that at 28 °C, according to SPR absorbance. Based on the study by Li, temperature can significantly affect fungal growth rate and metabolic activity.[47] In the literature, *P. pimiteouiense* growth was described to have an optimum growth at 17–28 °C. [48] In this study, the optimal temperature for the production of CuO NPs was 18 °C, which is similar to the environmental temperature at which this fungus was isolated. These results suggest that the initial pH of the medium and temperature can play major roles in fungal enzymatic and metabolic activities for the synthesis of CuO NPs.[45, 48, 49] It is also noteworthy to mention that SPR band correlates with the size and shape of the NPs produced.[50, 51] In our study, there was no significant change in the SPR band under different pH values (pH 7 and 10) and temperatures (18 °C and 28 °C) (Figure S4). This result indicates that the primary morphology of CuO NPs under these conditions did not change.

From the overall results, the optimal conditions to produce secreted enzymes for the CuO NPs synthesis were found to be at 18 °C, pH 7, and 5 mM Cu^{2+} dosage from a 10-day-old culture for this fungus. This optimum condition was further evaluated to determine the reaction time for the biosynthesis of CuO NPs (Figure 4 and Figure S5). The kinetics of the reaction indicate that the synthesis of CuO NPs was fast and almost complete in about 10 min. This result is much faster than previously reported fungus synthesizing metallic nanoparticles (1 h to 24 h).[52] The high efficiency in producing nanoparticles (high reaction rate and SPR peak) might be due to the larger amounts of proteins and biomolecules secreted by *P. pimiteouiense*.[17] This finding suggests that this microorganism is a good candidate for the green synthesis of CuO NPs.

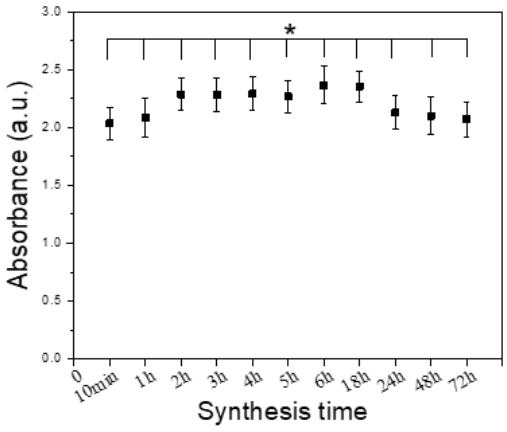

Figure 4. Amount of time for the synthesis of CuO NPs. The figure represents the UV-vis analysis over 72 h at wavelength 330 nm. Error bars represent mean standard deviations. UV-vis assay of three replicates of different synthesis times was analysed with a student's t-test. * P > 0.05 indicates no significant differences with different synthesis times from 10 min to 72 h. The spectra with the 330 nm peak, characteristic peak of CuO NPs at 18 °C, pH = 7, and 5 mM Cu^{2+} are presented in the supporting information (Figure S5).

Physico-chemical characteristics of CuO NPs

The nanoparticles synthesized under optimum conditions were harvested and fully characterized. Figure 5a shows the XRD results of two samples: commercial CuO NPs (chemically synthesized) and biosynthesized CuO NPs after repeated washing. The commercial CuO particles were highly crystalline and presented the typical *C2/c* symmetry that corresponds to a monoclinic crystalline structure. The characterization of this phase matched the JCPDS 801916 chart.[53] Similarly, these CuO characteristics have been observed by other research groups.[54, 55] On the other hand, the biosynthesized CuO NPs had a rather amorphous appearance with a broad peak. This has also been reported in the literature for other biosynthesized CuO particles.[33] The amorphous biosynthesized nanostructures may be the result of proteins around the nanoparticles acting as capping agents during the CuO NPs synthesis as described in Section 3.4. The characteristic peaks of biosynthesized CuO NPs were at 2θ of 23.5 and 42.7 (plane 014 and 050) (Figure 1a). These peaks matched previous reports for biosynthetic orthorhombic CuO NPs.[33] These results showed that the fungus was able to successfully biosynthesize CuO NPs.

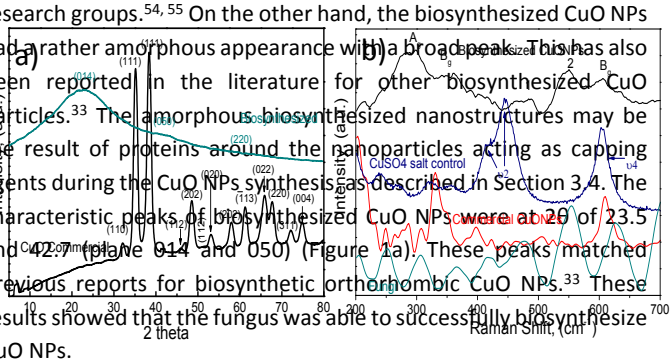

Figure 5. Characterization of the commercial and biosynthesized CuO nanoparticles. a) XRD for the commercial CuO nanoparticles and the biosynthesized CuO, and b) Raman spectroscopy analysis for the fungus, $CuSO_4$, commercial CuO, and biosynthesized CuO. The curves from top to bottom: 1- Biosynthesized CuO nanoparticles @ 18 °C, pH 7, and 5 mM Cu^{2+} dosage, 2- $CuSO_4$ salt control, 3- Commercial CuO nanoparticles, and 4- Freeze dried fungus grown on MYGP medium.

To further characterize the CuO NPs, Raman spectroscopy was also carried out (Figure 5b). The Raman for the fungal supernatant and $CuSO_4$ represented controls for any unexpected peaks in the biosynthetic CuO NPs to be subtracted. The $CuSO_4$ spectrum was well characterized by two main regions. The region below 400 cm^{-1} is associated with lattice phonons and was assigned to the internal modes of the compound. The region above 400 cm^{-1} is associated with the vibration modes for the SO_4.[56-58] These modes observed in our spectrum for $CuSO_4$ at 413, 425, and 448 cm^{-1} were symmetric bending (U_2) vibrational modes for SO_4^{2-}. The band identified at 607 cm^{-1} is the asymmetric bending (U_4).[57]

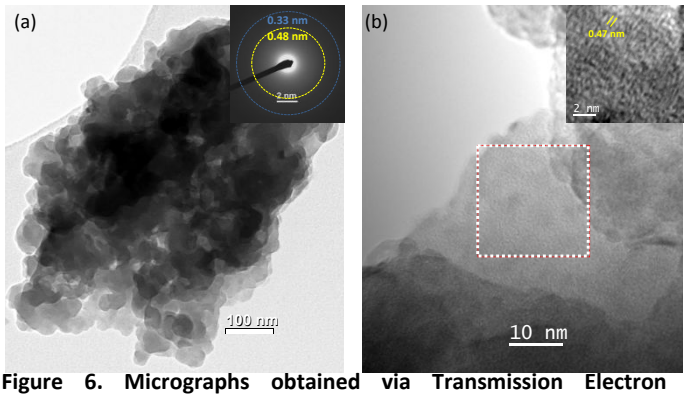

Figure 6. Micrographs obtained via Transmission Electron Microscopy. (a) bright field, and **(b)** high resolution. In both cases, the patterns agree that the structure is amorphous. The inset in **(a)** is the selected area for electron diffraction pattern (SAEDP) analysis and the one in **(b)** is a zoom-in from the dotted square. Both demonstrate the limited crystallinity of the CuO species.

On the other hand, the commercial CuO NPs presented three Raman active modes that were: one A_g and two B_g. The biosynthesized CuO had the same modes but was slightly shifted. This shift could be due to bio-products attached to the CuO nanoparticles. The A_g mode was at 282 and the other two B_g modes were at 333 and 626 cm^{-1}. There was a clear shift from the $CuSO_4$ into CuO observed in the spectra. This change was exhibited by the complete elimination of the symmetrical (U_2) and asymmetrical (U_4) vibrational modes of SO_4^{2-}. The two peaks (1 and 2) found in the biosynthetic nanoparticles are presumably related to biomolecules from the fungal supernatant. The noise-to-signal level in the biosynthesized sample was larger than in the other samples, which was attributed to two main reasons: (i) organic residue (e.g. biomolecules from the fungal secretions) and (ii) the poor crystallinity of the sample. Therefore, we can conclude that the XRD and Raman agree and demonstrate the presence of CuO with limited atomic range order. [59] Even if the biosynthesized nanoparticles exhibited a low crystallinity, amorphous CuO nanoparticles have been described to present more oxygen vacancies and display n-type conductivity, making them favourable for adsorption or electrical applications.[60, 61]

To further confirm the presence of amorphous CuO NPs from the synthesis, Figure 6 shows TEM results under a bright field (Figure 6a) and high-resolution transmission electron microscopy (HRTEM). In the bright field, the nanoparticles present an average size of 50 to 60 nm. Note that the aggregation of the particles observed in Figure 6 is mainly due to microscopy preparation. The HRTEM image clearly showed that the material is non-crystalline, having a rather amorphous nature. This observation was further confirmed by the selected area electron diffraction pattern (SAEDP) presented in the insets. The SAEDP is in good agreement with the HRTEM image presented in Figure 6b where the amorphous nature is evident. Overall, both images and the diffraction patterns support the XRD observations. A similar amorphous structure was also observed by other groups. The selected area for the electron diffraction pattern (SAEDP) is added to Figure 6a to show the diffused halos, typical of particles with limited crystallinity. The "rings" in the SAEDP match well with the interplanar distances for the planes (100) and (010) with respective $d_{(100)}$ = 0.48 nm and $d_{(010)}$ = 0.33 nm. The values are within a 2% difference to that of theoretical values and it is considered within the systematic error. The most important point here is to demonstrate that the particles have a similar crystalline structure to that seen in CuO with limited crystallinity as expected from the XRD results. Because it has more oxygen vacancies and displays n-type conductivity due to defects like dangling and floating bonds, amorphous CuO NPs are a good option for applications such as electrical, optical, and gas sensing applications.[60, 61]

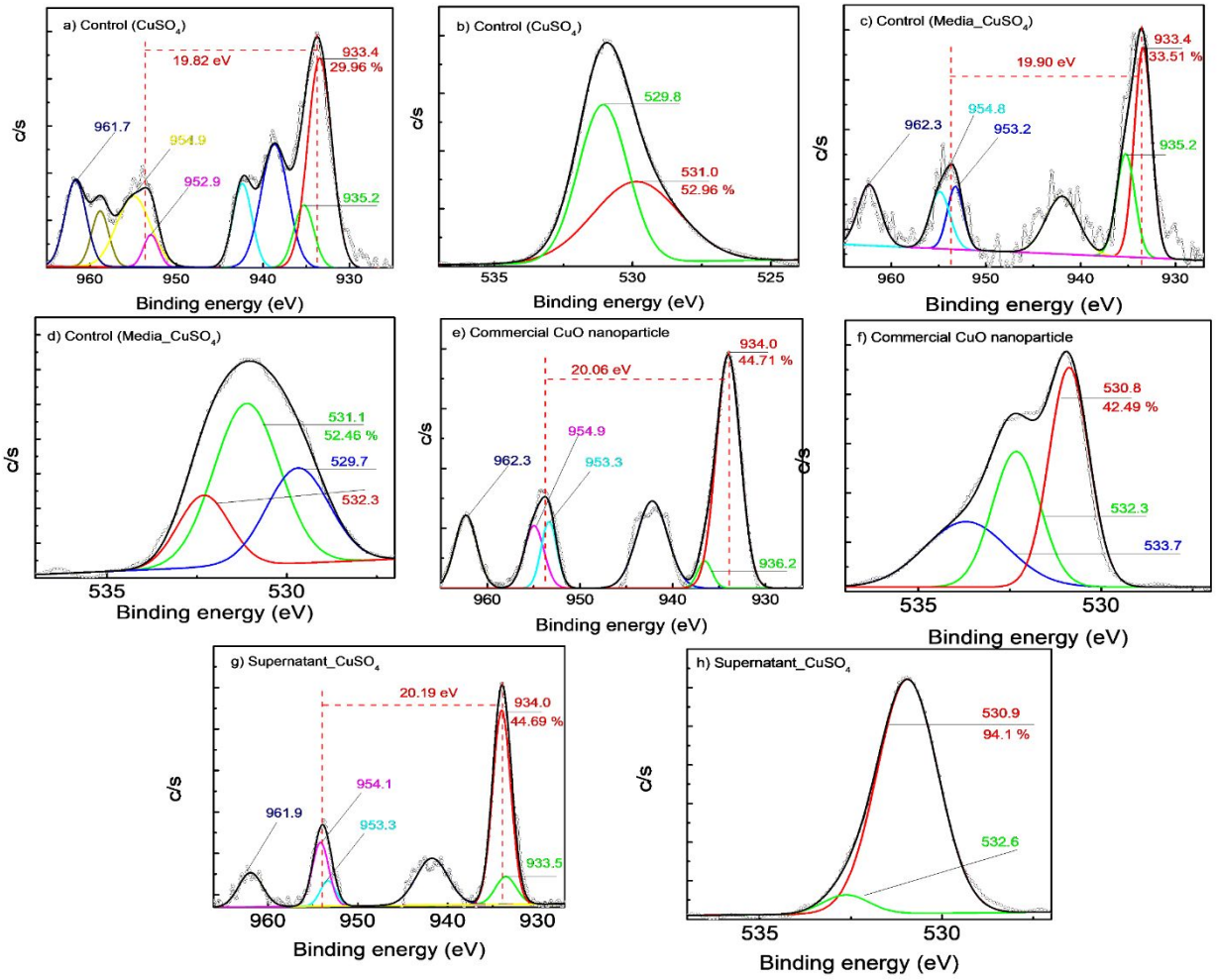

Figure 7. X-ray Photoelectron spectroscopy (XPS) analysis characterization. **(a)** control $CuSO_4$ (Cu2p), **(b)** control $CuSO_4$ (O1s), **(c)** control media + $CuSO_4$ (Cu2p), **(d)** control media + $CuSO_4$ (O1s), **(e)** control commercial CuO (Cu2p), **(f)** control commercial CuO (O1s), **(g)** supernatant_$CuSO_4$ (biosynthesized CuO) (Cu2p) and, **(h)** supernatant_$CuSO_4$ (biosynthesized CuO) (O1s).

The successful biosynthesis of CuO NPs was also confirmed by surface analysis using XPS (Figure 7). The control spectra with $CuSO_4$ salt only and media with Cu^{2+} only showed that the significant peaks at 933.4 eV and the binding energy separation of Cu ($2p_{3/2}$) and Cu ($2p_{1/2}$) peaks were 19.82 eV and 19.90 eV, respectively (Figure 7a and 7c). These results indicated that most of the phases in these controls were metallic Cu. Previous studies reported that a separation below or close to 19.8 eV corresponded to the pure metallic Cu phase.[62] On the other hand, the commercial CuO and biosynthesized CuO (Figures 7e and 7g) exhibited a significant peak at 934.0 eV, which corresponds to the peak of CuO.[63, 64] In addition, the separation of the binding energy was greater than 20 eV for CuO and biosynthesized CuO (Figures 7e and 7g), which indicated the presence of CuO.[65] In the case of oxygen bonding, the spectra of commercial and biosynthesized CuO were observed with the highest abundance at 530.8 eV and 530.9 eV. These peaks have been previously reported to correspond to the CuO phase.[66, 67] These XPS results confirm the successful production of biosynthetic CuO NPs by the fungus and further confirm the data obtained from the XRD, Raman, and TEM.

Role of Secondary Metabolites in CuO NP Formation

Fungi are known to secrete substantial quantities of reductases, proteins, and secondary metabolites. Previous studies showed that certain enzymes were involved in the production of Au and Ag nanoparticles (NPs).[17, 18] Besides NAD(P)H-dependent reductases mentioned above,[68] some other researchers also reported the roles

of hydrolyses, such as amylases, xylanases, and proteases in the production of metal and metal-oxide NPs.

Apart from the reductases and hydrolyses mentioned above, various secondary metabolites (such as polyphenols, phenolic acid and terpenoids, organic acids, and other biomolecules) produced in metabolic pathways have also been reported to significantly contribute to both the reduction and stabilization of metallic NPs in the intricate redox biosynthesis processes of bacteria, fungi, and plant extracts.[69, 70] However, there is still a lack of a systematic study to understand the mechanistic aspects of metabolic products and key enzymes playing a role in CuO NP synthesis. Herein, we first performed a differential metabolomics investigation with the fungus growing in MYGP and PDB by using LC-MS/MS to collect the metabolomics raw data, followed by Thermo Compound Discoverer™ software and KEGG pathway analyses to identify the main secondary metabolites contributing to NP production. Secondly, the non-target LC-MS/MS-based metabolite profile was analysed by comparing the supernatant of the fungus grown in both MYGP medium (CuO NPs producing condition) and PDB medium (without CuO NPs producing condition) to determine the different metabolites secreted in each growth medium. The final differential analysis results (shown as a 'Volcano plot,' Figure 8) showed distinct differences between the two growth media, where *P. pimiteouiense* secreted a more significant number of metabolites (257 metabolites) when grown in MYGP than in PDB (33 metabolites). These results highlight the variations in metabolic excretion based on the culture media. The results strongly suggested that the metabolites secreted exclusively in MYGP medium (absent in PDB medium) were associated with CuO NPs formation.

To gain a deeper understanding of the specific roles of the unique metabolites found in the MYGP sample (Figure 8), the metabolites were cross-referenced with the KEGG pathway database. Through the database, it was possible to determine the association of the metabolites with oxidoreductases and corresponding metabolic pathways. Table 1 presents several key NADPH-dependent oxidoreductases and their associated metabolic reaction pathways. The six differentially expressed secondary metabolites exclusively expressed in the MYGP medium (including Hydroxyquinol, 2-hydroxy-2-methylbutanenitrile,5a,11a-Dehydrooxy-tetracycline, Thymidine, L-Valine o-Hydroxylamino-benzoate) are part of several metabolic reactions (such as Cyanoamino acid metabolism) involving multiple NADPH-dependent oxidoreductases. These reactions are known to yield NADPH co-factors in their metabolic pathways as illustrated in Figure 9.

The role of the reductases identified earlier in this study for the synthesis of CuO NPs and the identification of NADPH/$NADP^+$ pairs and NADPH-dependent oxidoreductases (including NADPH cofactors) in the metabolomics analysis suggests that these metabolic molecules are playing a crucial role as electron donors for the reduction of Cu^{2+} to nanoparticles and concurrently oxidizing to CuONPs through electron transportation and redox reactions. Furthermore, as shown in Table S2, certain relevant oxidases, which are responsible for oxidation reactions, were present in the MYGP sample only. Previous studies suggested that O_2 (from aerobic culture) or certain oxidants produced by oxidases[71]are also responsible for the concurrent formation of CuO NPs.[72, 73]

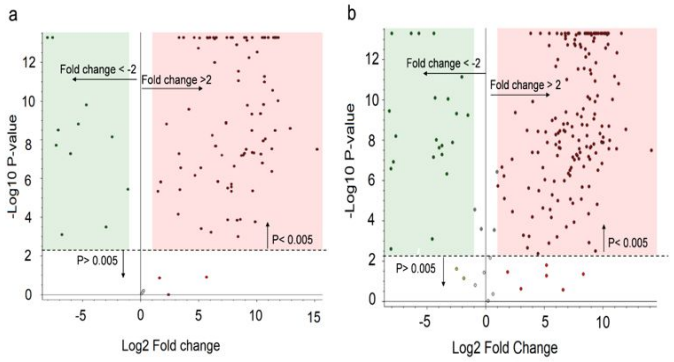

Figure 8. Volcano plots of fungal metabolites (total 257 components and 34 components from MYGP and PDB growth media, respectively) from the differential analysis between the two cultures (MYGP vs.PDB). (a) Negative ion mode (ESI (-) compounds identified: 11 compounds from PDB growth media and 88 compounds from MYGP growth media and, **(b)** Positive ion mode (ESI (+) compounds identified: 22 compounds from PDB and 169 compounds from MYGP. X-axis shows the fold change (FC) in intensity on a log 2 scale (fungi supernatant/ medium matrix). Each circle represents a different metabolite compound. The metabolites in MYGP and PDB medium are marked with red and green circles, respectively. The vertical solid line indicates the two-fold change threshold (up (FC > 1) or down (FC < -1), to visualize the compounds that are significantly increased in MYGP and PDB medium.

In addition to the presence of these oxidoreductases secreted in the MYGP during the fungal growth, certain secondary metabolites featuring two phenolic groups are also produced by the unique fungal metabolism in the MYGP medium (Table S3 and S4). These biomolecules with two phenolic groups (such as ortho-, para-) can reduce Cu^{2+} ions, given the favourable reduction potential (0.340 V vs. SCE - saturated calomel electrode), and promote the formation of CuO NPs. This fungus, compared to other fungal species that rely solely on reductases as reductants, has also secondary metabolites with multiple phenolic groups that can function as electron donors and participate in redox. These multiple bio-reductases probably explain the much more rapid synthesis rate of CuO NPs (production of NPs within 10 min) when compared to other fungi species.[52] Rarely has fungal synthesis of metallic NPs been thoroughly examined to also identify compounds with phenolic groups present in the secreted metabolites, as shown in this study. Previous studies with plant extracts have shown that metabolites containing multiple phenolic groups possess a strong chelating ability with metal ions, enabling them to participate in nucleation and the formation of well-structured CuO aggregates following the nucleation and growth mechanisms of NP formation.[74-76] Consequently, by identifying the presence of compounds with phenolic groups in the secondary

metabolites of this fungus, we further validate the pivotal role of secondary metabolites with multiple phenolic groups in *P. pimiteouiense* bio-redox, nucleation, and the formation of CuO NPs, alongside the bio-redox mediated by NADPH reductases mentioned earlier, culminating in the production of NPs.

To substantiate the roles of these secondary metabolites in the CuO NPs synthesis, FTIR spectroscopy was employed to identify functional groups on the CuO NPs' surface responsible for the bio-reduction and stabilization of CuO NPs. In the IR spectrum of the CuO NPs, we observed a broad, aromatic H-bonded -OH stretch at 3229 cm^{-1}, a weak aromatic C=C stretch at 1546 cm^{-1} and 2929 cm^{-1}, representing phenolic groups.[77] Notably, the distinct shifts and reductions corresponding to the stretching vibrations of hydroxyl from 3302 cm^{-1} (as observed in the supernatant control, Figure S6) to 3329 cm^{-1} revealed that CuO NPs formation and stabilization involve secondary metabolites with phenolic groups, as observed in the volcano plot (such as digallic acid). The presence of protein functional groups at 1450 cm^{-1}, 1650 cm^{-1}, 1398 cm^{-1}, and 1123 cm^{-1} provides evidence of the existence of bending vibrations in aromatic ring compounds, amide I and II stretching vibrations in the amide groups of proteins, and C-N stretching of amines, respectively.[78, 79] Similarly, the peaks corresponding to the C-N stretch of amines shift and decrease from 1078 cm^{-1} (in the supernatant) to 1123 cm^{-1} indicate that amide groups binding to the CuO NPs' surface as capping agents, which is consistent with Pimprikar et al.[80] Phenolic and amides have been previously described as bio-redox and capping agents for biogenic Au and Ag NPs.[81, 82] The role of secondary amide derivatives as capping agents was reported for spherical Ag NPs or Au NPs (< 30nm) biosynthesis using fungi,[83] bacteria,[84] and plant extracts.[85] Our results revealed that secondary metabolites with multi-phenolic and amide groups also possess these dual roles for CuO NPs synthesis by fungi. Here the spherical shape and stability of biogenic CuO NPs seems to be due to amide groups *as confirmed by our FTIR results*.

Moreover, the freshly biosynthesized CuO NPs dispersed in $NaNO_3$ solution exhibited a negatively charged ζ-potential, consistent with reports from other research groups on biosynthetic CuO NPs. Particles with ζ-potential values ranging from ±10 to ±20 mV and over 20 mV indicate the formation of stable nanoparticles.[86] These results unequivocally confirmed that secondary metabolites such as multiple phenolic groups and peptides are responsible for the stabilization of CuO NPs. [87, 88] These metabolites bind to the surface of NPs primarily through phenolic hydroxy groups and free amines, ensuring the final formation of CuO NPs with consistent shape and size observed in our TEM.

To summarize, the synthesis of CuO NPs by *P. pimiteouiense* can be delineated through the following key steps (Figure 9). Firstly, suitable growth media, such as MYGP, and suitable growth conditions are necessary to stimulate the synthesis of multi-NADPH-dependent oxidoreductases and secondary metabolites containing multiple phenolic groups (at least two -OH groups) that act as electron donors, facilitating the conversion of Cu^{2+} to CuO. Finally, secondary metabolites with phenolic and amide groups, as revealed by FTIR analysis, act as capping agents, leading to the thermodynamic stability of CuO NPs with a defined shape and size.

Conclusions

In conclusion, this study presents a straightforward, rapid, and sustainable approach for the bio-fabrication of CuO NPs under ambient conditions. This work also demonstrates for the first time the capability of *P. pimiteouiense,* a fungal isolate from a copper mine, to biosynthesize CuO NPs. The successful extracellular synthesis of CuO NPs was influenced by different parameters: initial medium pH, temperature, copper ion concentration, as well as fungal growth phase, and culture media. Under optimized conditions, *P. pimiteouiense* achieves a swift synthesis (producing CuO NPs within 10 minutes) of CuO NPs. Metabolomic analysis indicated the presence of specific NADPH oxidoreductases and NADPH cofactors as the dominant

Table 1. The representative NADPH dependent oxido-reductases differentially secreted in MYGP culture medium after the growth of the fungus.

Metabolites linked to NADPH- dependent Oxido-reductases	Formula	Potential related KEGG (or BioCyc) metabolism Pathway	Enzyme
Hydroxyquinol	$C_6H_6O_3$	Microbial metabolism in diverse environments /Benzoate degradation	**NADPH cofactor:** Resorcinol 4-hydroxylase (NADPH) (EC1.14.13.219)
2-hydroxy-2-methylbutanenitrile	C_5H_9NO	Biosynthesis of secondary metabolites, Cyanoamino acid metabolism	(E)-2-methylbutanal oxime monooxygenase (EC 1.14.14.41)
5a,11a-Dehydrooxy-tetracycline	$C_{22}H_{22}N_2O_9$	Tetracycline biosynthesis Or Biosynthesis of type II polyketide products	5a,11a-dehydrotetracycline 5-monooxygenase (EC1.14.13.234)
o-Hydroxylamino-benzoate	$C_7H_7N\ O_3$	Microbial metabolism in diverse environments, Aminobenzoate degradation	NA
Thymidine	$C_{10}\ H_{14}\ N_2\ O_5$	Reported as electron donor by NADPH enzyme reaction	NA
L-Valine	$C_5\ H_{11}\ N\ O_2$	Biosynthesis of secondary metabolites, Cyanoamino acid metabolism, Glucosinolate biosynthesis	Valine N-monooxygenase (EC 1.14.14.38) Isoleucin N-monooxygenase

mechanisms for providing electron donors to Cu^{2+} and conversion of CuO NPs. Furthermore, secondary metabolites containing phenolic compounds (with multi-hydroxyl (-OH) groups) were confirmed to play additional roles in the biosynthesis process of CuO NPs. Specific oxidases, which can lead to the production of oxidants or O_2 from aerobic growth culture, were also suggested for the formation of CuO NPs. The capping and stabilization of the nanoparticles were also determined to involve amides, proteins, and phenolic molecules.

This study contributes to a deeper understanding of the biosynthetic pathway of metallic NPs through a physiological and metabolomic approach. This investigation also provides a new opportunity for developing green synthesis of metal oxide nanoparticles for potential larger-scale applications. To achieve this goal, our future research in CuO NPs manufacturing will focus on investigating the life cycle assessment (LCA) to compare different synthesis routes (such as chemical vs. biosynthesis) to assess their yield (synthesis efficiency), sustainability, environmental impacts (such as greenhouse gas emission) and energy demand. By incorporating these insights, we will be able to confirm that this process provides a green and sustainable synthesis of CuO NPs and determine the feasibility of scaling up the production and commercialization of these nanoparticles.

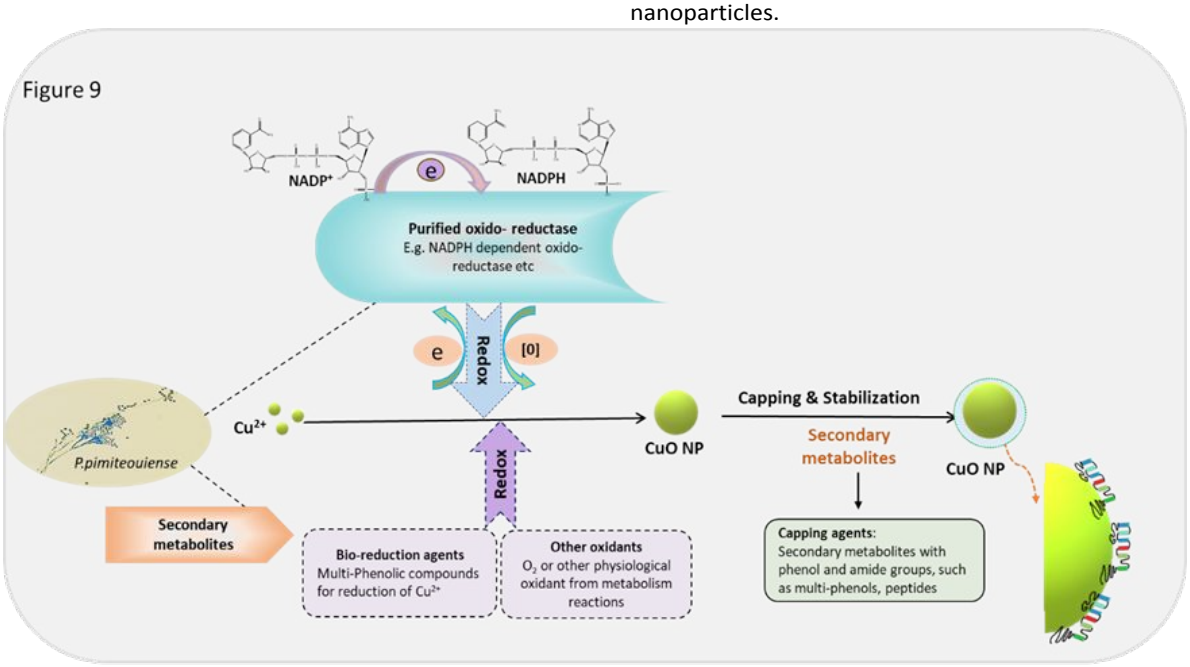

Figure 9: Schematic illustration of the possible formation mechanism of CuO NPs. The purified NADPH oxidoreductases and secondary metabolites (such as multi-phenol groups) identified in our study jointly contribute to the rapid biosynthesis of CuO NPs. NADPH-dependent oxidoreductase enzymatic reactions involve donating electrons to copper ions and concurrent oxidation of CuO NPs (the metabolites from MYGP serving as substrates or products of the reaction, as determined by pathway analysis; detailed electron transfer reactions are provided in the supporting information). Additionally, either O_2 or oxidants produced during oxidative enzymatic reactions are involved in the final formation of CuO NPs (the possible oxidase responsible for producing oxidants is presented in the supporting information).

Conflicts of interest

There are no conflicts to declare.

Acknowledgments

This project was supported by the National Science Foundation Award Number: 2125480, the U.S. Department of Energy: Biological and Environmental Research Science Focus Area grant (grant no. DE-AC52-06NA25396), and the Welch Foundation Center for Advanced Bioactive Materials Crystallization (Grant No. V-E-0001). The findings achieved herein are solely the responsibility of the authors.

References

[1]. Montgomerya MJ, Sugaka N, Yangb. KR. Semiconductor-to-conductor transition in 2D copper (II)

oxide nanosheets through surface sulfur-functionalization. Nanoscale. 2020;12:14549-59
[2]. Mayer KM, Hafner JH. Localized Surface Plasmon Resonance Sensors. Chem Rev. 2011;111(6):3828–57.
[3]. Meng J, Yang. h, Chen. L, Qin. H, Cui. F, Jiang. Y, et al. Energy storage performance of CuO as a cathode material for aqueous zinc ion battery. Materials Today Energy. 2020;15:1-8.
[4]. Lekbach Y, Dong Y, Li Z, Xu D, Abed SE, Yi Y, et al. Catechin hydrate as an eco-friendly biocorrosion inhibitor for 304L stainless steel with dual-action antibacterial properties against Pseudomonas aeruginosa biofilm. Corrosion Science. 2019;157(15):98-108.
[5]. Lv Y, Liua J, Zhang Z, Zhang. W. Green synthesis of CuO nanoparticles-loaded ZnO nanowires arrays with enhanced photocatalytic activity. Materials Chemistry and Physics.267:124703.
[6]. Kampmann J, Betzler S, Hajiyani H, Häringer. S. How photocorrosion can trick you: A detailed study on low bandgap Li doped CuO photocathodes for solar hydrogen production. Nanoscale. 2020;12:7766-75.
[7]. Sivayogam D, Punithavathy IK, Jayakumar. SJ. Study on structural, electro-optical and optoelectronics properties of CuO nanoparticles synthesis via sol gel method. Materials Today: Proceedings.In press.
[8]. Ostrowski J, Wu JY, Rueger DC, Miller BE, Siegel LM, NM. K. Characterization of the cysJIH regions of Salmonella typhimurium and Escherichia coli B. DNA sequences of cysI and cysH and a model for the siroheme-Fe4S4 active center of sulfite reductase hemoprotein based on amino acid homology with spinach nitrite reductase. J Biol Chem. 1989 264(26):15726-37.
[9]. Singh DP, Ojha AK, Srivastava. ON. Synthesis of different Cu (OH) 2 and CuO (nanowires, rectangles, seed, belt, and sheetlike) nanostructures by simple wet chemical route. J Phys Chem C. 2009;113:3409-18.
[10]. Katwal R, Kaur H, Sharma G, Naushad M, Pathania. D. Electrochemical synthesized copper oxide nanoparticles for enhanced photocatalytic and antimicrobial activity. J Industrial Eng Chem 2015;31:173–84.
[11]. Son DI, You CH, Kim. TW. Structural, optical, and electronic properties of colloidal CuO nanoparticles formed by using a colloid-thermal synthesis process. Appl Surf Sci. 2009;255:8794-7.
[12]. Abdel-Monem YK, S.M. Emam HMO. Solid state thermal decomposition synthesis of CuO nanoparticles from coordinated pyrazolopyridine as novel precursors. J Mater Sci Mater Electronics. 2017;28(3):2923–34.
[13]. Karunakaran C, Magesan P, Gomathisankar P, Vinayagamoorthy. P. Absorption, photoluminescence and photoelectron transfer resistance of sol–gel synthesized core/shell CuO/TiO2 nanoparticles. Optik-International Journal for Light and Electron Optics. 2016;127:3013-7.
[14]. Arun K, Batra A, Krishna A, Bhat K, Aggarwal M, Francis. PJ. Surfactant free hydrothermal synthesis of copper oxide nanoparticles. American J Mater Sci 2015;5(3A):36–8.
[15]. Rajesh R, Matthew RF, Anthony P OM, Peter MS, Suresh KB, Vipul B, et al. Aqueous phase synthesis of copper nanoparticles: a link between heavy metal resistance and nanoparticle synthesis ability in bacterial system. Nanoscale. 2013;5:2300-7.
[16]. Gracioso LH, Pena-Bahamonde J, Karolski B, Borrego BB, Perpetuo EA, do Nascimento CAO, et al. Copper mining bacteria: Converting toxic copper ions into a stable single-atom copper. Sci Adv. 2021;7(17).
[17]. Siddiqi KS, Husen A. Fabrication of metal nanoparticles from fungi and metal salts: Scope and application. Nanoscale research letters. 2016;11:1-15.
[18]. Kitching M, Ramani M, Marsili E. Fungal biosynthesis of gold nanoparticles :mechanism and scale up. Microb Biotechnol. 2015;8:13.
[19]. Zhao X, Zhou LF, Rajoka MSR, Yan L, Jiang C, Shao D. Fungal silver nanoparticles: synthesis,application and challenges: synthesis, application and challenges. Critical reviews in biotechnology. 2018;38(6).
[20]. Sanghi R, Verma P, Puri S. Enzymatic Formation of Gold Nanoparticles Using Phanerochaete Chrysosporium. Advances in Chemical Engineering and Science. 2011;01:154-62.
[21]. Gopinath K, Arumugam A. Extracellular mycosynthesis of gold nanoparticles using Fusarium solani. Applied Nanoscience. 2014;4(6):657-62.
[22]. Narayanan KB, Sakthivel N. Biological synthesis of metal nanoparticles by microbes. Adv Colloid Interface Sci. 2010;156:1-13
[23]. Korbekandi H, Siavash I, Abbasic S. Optimization of biological synthesis of silvernanoparticles using Lactobacillus casei subsp.casei. J Chem Technol Biotechnol 2012;87:932-7.
[24]. Pitt J, Hocking AD. Fungi and Food Spoilage. Blackie Academic and Professional L, England, editor2009,3rd Ed. 519-32 p.
[25]. Refai M, El-Yazid., A. H, Tawakkol W. Monograph on the genus Penicillium: A guide for historical, classification and identification of penicilli, their

industrial applications and detrimental effects. 24 ed. University of Cairo2015.
[26]. White TJ, Bruns T, Lee S, Taylor J. Amplification and Direct Sequencing of Fungal Ribosomal RNA Genes for Phylogenetics. In: Innis, M.A., Gelfand, D.H. and Sninsky, J.J., Eds., PCR Protocols: A Guide to Methods and Applications,New York.1990. 315-22 p.
[27]. De Hoog GS, Gerrits van den Ende AH. Molecular diagnostics of clinical strains of filamentous Basidiomycetes. Mycoses. 1998;41:183-9.
[28]. Liang X, Yang Y, Jin X, Huang Z, Kang F. The high performances of SiO2/Al2O3-coated electrospun polyimide fibrous separator for lithium-ion battery. Journal of Membrane Science. 2015;493:1-7.
[29]. Parikh D, Jafta CJ, Thapaliya BP, Sharma J, Meyer HM, Silkowski C, et al. Al2O3/TiO2 coated separators: Roll-to-roll processing and implications for improved battery safety and performance. Journal of Power Sources. 2021;507:230259.
[30]. Liu H, Wan HQ. Separation & purification of Sulfite Reductase and study on Its Zymological Properties Liquor-making Science &Technology. 2006;6:28-31.
[31]. Jiang ST, ML. H, SH. J, HC. C, HC. C, HC. C. Purified NADPH-sulfite reductase from saccharomyces cerevisiae effects on quality of ozonated mackerel surimi J Food Sci 1998a;63:777-81.
[32]. Nguyen HN, Nadres ET, Alamani BG, Rodrigues DF. Designing polymeric adhesives for antimicrobial materials: poly (ethylene imine) polymer, graphene, graphene oxide and molybdenum trioxide–a biomimetic approach. Journal of Materials Chemistry B 2017;5(32):6616-28.
[33]. Jadhavetc MS. Green biosynthesis of CuO&Ag–CuO nanoparticles from Malus domestica leaf extract and evaluation of antibacterial, antioxidant and DNA cleavage activities. New J Chem. 2018;42:204-13.
[34]. Millstone JE, Hurst SJ, Métraux GS, Cutler JI, Mirkin CA. Colloidal gold and silver triangular nanoprisms. Small (Weinheim an der Bergstrasse, Germany). 2009;5(6):646-64.
[35]. Petit C, Lixon P, Pileni MP. In situ synthesis of silver nanocluster in AOT reverse micelles. The Journal of Physical Chemistry. 1993;97(49):12974-83.
[36]. Petit C, Lixon P, Pileni MP. In Situ Synthesis of Silver Nanocluster in AOT Reverse Micelles. J Phys Chem. 1993 97(49):12974 - 83
[37]. Arumugam KGA. Extracellular mycosynthesis of gold nanoparticles using Fusarium solani. Appl Nanosci 2014;4:657-62.
[38]. Mohammadhassan GS, Zeynab G-S, Akbarzadeh A, Zeynab G-S, Akbarzadeh A, Zeynab G-S, et al. Enzymatic synthesis of gold nanoparticles using sulfite reductase purified from Escherichia coli: A green eco-friendly approach Process. Biochemistry. 2015;50:1076-85.
[39]. Skowronski BS, Gottlieb D. Age-dependent metabolic differences in peripheral hyphae of Rhizoctonia solani. Journal of bacteriology. 1970;104:640-5.
[40]. Baldrian P, Der Wiesche C, Gabriel J, Nerud F, Zadrazil F. Influence of cadmium and mercury and activities of ligninolytic enxymes and degradation of polycyclic aromatic hydrocarbons by Pleurotas ostreatus. ApplEnviron Microbiol. 2000. ;66:2471-8.
[41]. Ruiz B, Chávez A, Forero A, García-Huante Y, Romero A, Sánchez M, et al. Production of microbial secondary metabolites: regulation by the carbon source. Critical reviews in microbiology. 2010;36(2):146-67.
[42]. R. Cuevas N, Durán MC, Diez GR, Tortella OR. Extracellular Biosynthesis of Copper and Copper Oxide Nanoparticles by Stereum hirsutum, Native White-Rot Fungus from Chilean Forests. Journal of Nanomaterials. 2014;2015.
[43]. Ramanathan R, Field MR, O'Mullane AP, Smooker PM. Aqueous phase synthesis of copper nanoparticles: a link between heavy metal resistance and nanoparticle synthesis ability in bacterial systems. Nanoscale. 2013;5:2300–6.
[44]. Pimprikar PS, Joshi SS, Kumar AR, Zinjarde SS, Kulkarni SK. Influence of biomass and gold salt concentration on nanoparticle synthesis by the tropical marine yeast Yarrowia lipolytica NCIM 3589. Colloids and Surfaces B: Biointerfaces. 2009;74(1):309-16.
[45]. Kim BW, Kwon HJ, Park HY, Nam SW, Park JP, Yun JW. Production of a novel transfructosylating enzyme from Bacillus macerans EG-6 Bioprocess Engineering 2000;23:11-6
[46]. Srinivasan S, Rani P. Biological synthesis of copper nanoparticles using Pseudomonas fluorescens. IntJCurrMicrobiolAppSci, . 2014;3:374-83.
[47]. Li Y, Wadso L, Larsson L. Impact of temperature on growth and metabolic efficiency of Penicillium roqueforti -correlations between produced heat, ergosterol content and biomass. Journal of Applied Microbiology. 2009;106:1494-501.
[48]. Cao C, R.L. ZW, Wei L, Wang. X, Qiao. J, Wang. D, et al. The effects of temperature, pH and salinity on the growth and dimorphism of penicillium marneffei. Medical Mycology. 2007;71:401-7.

[49]. Narendranath NV, Power R. Relationship between pH and medium dissolved solids in terms of growth and metabolism of lactobacilli and saccharomyces cerevisiae during ethanol production. Appl Environ Microbiol. 2005;2239-2243.
[50]. Petit.C., Lixon P, Pileni MP. In Situ Synthesis of Silver Nanocluster in AOT Reverse Micelles. J Physical Chemistry 1993;97:12974-83.
[51]. Velgosová O, Mražíková M, Marcinčákovác A. Influence of pH on green synthesis of Ag Nanoparticles. Materials Letters 2016; 180(1): 336-9
[52]. Dagher S, Haik Y, Ayesh AI, Tit N. Synthesis and optical properties of colloidal CuO nanoparticles. Journal of Luminescence. 2014;151:149-54
[53]. Azam A, Ahmed AS, Oves M, Khan MS, Memic A. Size-dependent antimicrobial properties of CuO nanoparticles against Gram-positive and -negative bacterial strains. Int J Nanomedicine. 2012;7:3527-35.
[54]. Ahmad R, Vaseem M, Tripathy N, Hahn YB. Wide linear-range detecting nonenzymatic glucose biosensor based on CuO nanoparticles inkjet-printed on electrodes. Anal Chem. 2013;85(21):10448-54.
[55]. Zhu JW, Li D, Chen HQ, Yang XJ, Lu L, Wang X. Highly dispersed CuO nanoparticles prepared by a novel quick-precipitation method. Materials Letters. 2004;58(26):3324-7.
[56]. Montero S, Schmölz R, Haussühl S. Raman spectra of orthorhombic sulfate single crystals I: K_2SO_4, Rb_2SO_4, Cs_2SO_4 and Ti_2SO_4. Journal of Raman Spectroscopy. 1974;2(1):101-13.
[57]. Fu X, Yang G, Sun J, Zhou J. Vibrational spectra of copper sulfate hydrates investigated with low-temperature Raman spectroscopy and terahertz time domain spectroscopy. J Phys Chem A. 2012;116(27):7314-8.
[58]. Mayer KM, Hafner JH. Localized surface plasmon resonance sensors. Chemical reviews. 2011;111(6):3828-57.
[59]. Chakraborty S, Das A, Begum MR, Dhara S, Tyagi AK, Tyagi. AK. Vibrational properties of CuO nanoparticles synthesized by hydrothermal technique. AIP Conference Proceedings. 2011;1349(1):841-2.
[60]. Tian Z, Bai H, Li Y, Liu W, Li J, Kong Q, et al. Gas-Sensing Activity of Amorphous Copper Oxide Porous Nanosheets. ChemistryOpen. 2020;9(1):80-6.
[61]. Parvathy T, Sabeer NAM, Mohan N, Pradyumnan PP. Effect of dopant gas pressure on the growth of magnetron sputtered CuO thin films for electrical and optical applications. Optical Materials. 2022;125:112031.
[62]. Shaikh JS, Pawar RC, Devan RS, Ma YR, Salvi PP, Kolekar SS, et al. Synthesis and characterization of Ru doped CuO thin films for supercapacitor based on Bronsted acidic ionic liquid. Electrochimica Acta. 2011;56(5):2127-34.
[63]. Ma H, Liu Y, Fu Y, Yu C, Dong X, Zhang X, et al. Improved photocatalytic activity of copper heterostructure composites (Cu–Cu_2O–CuO/AC) prepared by simple carbothermal reduction. AUST J CHEM. 2014;67:749.
[64]. Zhu X, Gupta K, Bersani M, A. Darr J, R. Shearing P, Brett DJL. Electrochemical reduction of carbon dioxide on copper-based nanocatalysts using the rotating ring-disc electrode. Electrochimica acta 2018;283:1037-44.
[65]. Shaikh JS, Pawar RC, Devan RS, Ma YR. Synthesis and characterization of Ru doped CuO thin films for supercapacitor based on Bronsted acidic ionic liquid. Electrochimica Acta. 2011;56(5):2127-34.
[66]. Wan WN, Che Ramli ZA, Hakim Lahuri A, Yusop R, Wahab M, Yarmo A. Enhancement of CO_2 capture using CuO nanoparticles supported on green activated carbon. Advanced Materials Research. 2015;1087:111-5.
[67]. Boruban C, Esenturk EN. Synthesis of CuO nanostructures on zeolite-Y and investigation of their CO_2 adsorption properties. Journal of Materials Research. 2017;32(19):3669-78.
[68]. Li Q, Li F, Li M, Chen C, GADD. GM. Nanoparticle and nanomineral production by fungi. Fungal Biology Reviews. 2022;41:31-44.
[69]. Ovais M, Khalil. AT. Plant phytochemicals and microbial enzymes in biosynthesis of metallic nanoparticles.
. Applied Microbiology and Biotechnology. 2018;101:6800.
[70]. Singh A, Singh NB, Hussain I, Singh H. Effect of biologically synthesized copper oxide nanoparticles on metabolism and antioxidant activity to the crop plants J. Biotechnol. 2017;262:11–27.
[71]. Waghchaure RH, Adole VA. Biosynthesis of metal and metal oxide nanoparticles using various parts of plants for antibacterial, antifungal and anticancer activity: A review. Journal of the Indian Chemical Society. 2023;100(5):100987.
[72]. Jeevanandam J. Biosynthesis of Metal and Metal Oxide Nanoparticles. ChemBio Eng Rev. 2016;2(55):55-67.
[73]. Sutradhar P. Microwave synthesis of copper oxide nanoparticles using tea leaf and coffee powder extracts and its antibacterial activity. Journal of

Nanostructure in Chemistry. J Nanostruct Chem. 2014;4:86.
[74]. Saif S, Tahir. A, Chen. Y, Chen. Y, Chen. Y. Green synthesis of iron nanoparticles and their environmental applications and implications. Nanomaterials. 2016;6:209.
[75]. Bogireddy NKR, Anand KKH, Mandal BK. Gold nanoparticles-Synthesis by Sterculia acuminata extract and its catalytic efficiency in alleviating different organic dyes. Journal of Molecular Liquids. 2015;211:868-75.
[76]. Xiong J, Wang Y, Xue Q, Wu X. Synthesis of highly stable dispersions of nano sized copper particles using l-ascorbic acid. Green Chem. 2011;13 900-4.
[77]. Singh A, Singh NB, Hussain I, Singh H. Effect of biologically synthesized copper oxide nanoparticles on metabolism and antioxidant activity to the crop plants Solanum lycopersicum and Brassica oleracea var. botrytis. Journal of Biotechnology. 2017;262:11-27.
[78]. Ahmad A. Biosynthesis of silver nanoparticles using the fungus Fusarium oxysporum. Colloids and Surfaces B: Biointerfaces. 2003;28:313-8.
[79]. Bankar AV, Kumar AR, Zinjarde SS. Removal of chromium (VI) ions from aqueous solution by adsorption onto two marine isolates of Yarrowia lipolytica. J Hazard Mater 2019;170:487–94.
[80]. Pimprikar PS, Joshi SS, Kumar AR, Zinjarde SS, Kulkarni SK. Influence of biomass and gold salt concentration on nanoparticle synthesis by the tropical marine yeast Yarrowia lipolytica NCIM3589. Colloids SurfB Biointerfaces 2009;74:309-16
[81]. Lin Z, Wu J, Xue R. Spectroscopic characterization of Au^{3+} biosorption by waste biomass of Saccharomyces cerevisiae. Spectrochim Acta A. 2005;61:761-5.
[82]. Jayaprakash M, Kannappan S. An overview of a sustainable approach to the biosynthesis of AgNPs for electrochemical sensors. Arabian Journal of Chemistry. 2022;15(12):104324.
[83]. Gudikandula K, Vadapally P, Singara Charya MA. Biogenic synthesis of silver nanoparticles from white rot fungi: Their characterization and antibacterial studies. OpenNano. 2017;2:64-78.
[84]. Alfryyan N, Kordy MGM, Abdel-Gabbar M, Soliman HA, Shaban M. Characterization of the biosynthesized intracellular and extracellular plasmonic silver nanoparticles using Bacillus cereus and their catalytic reduction of methylene blue. Scientific Reports. 2022;12(1):12495.
[85]. Sahayaraj K, Balasubramanyam G, Chavali M. Green synthesis of silver nanoparticles using dry leaf aqueous extract of Pongamia glabra Vent (Fab.), Characterization and phytofungicidal activity. Environmental Nanotechnology, Monitoring & Management. 2020;14:100349.
[86]. Kumari N, Mathe VL, Dongre PM. Albumin nanoparticles conjugates binding with glycan - A strategic approach for targeted drug delivery. Int J Biol Macromol. 2019;126(126):74-90.
[87]. Vasantharaj S, Sathiyavimal S, Saravanana M, Senthilkumar P, Gnanasekaran K, Shanmugavel M. Synthesis of ecofriendly copper oxide nanoparticles for fabrication over textile fabrics: Characterization of antibacterial actiivty and dye degradation potential. Journal of photochemistry &photobiology,B:Biology 2019;191:143-9.
[88]. Liu H, Lai W, Liu X, Yang H, Fang. Y, Fang. Y. Exposure to copper oxide nanoparticles triggers oxidative stress and endoplasmic reticulum (ER)-stress induced toxicology and apoptosis in male rat liver and BRL-3A cell. J Hazard Mater 2021;401(5):123349.

Data availability statements

- The authors declare that the data supporting the findings of this study are available within the paper and its supplementary Information files. Should any data files be needed in another format they are available from the corresponding author upon reasonable request.
- The finding in this manuscript including redox/ reductases etc metabolites and metabolic pathway etc are available at the following
  URL: **https://www.genome.jp/kegg/**

  For example:
  The underlying/extending info for NADPH dependent redox identified in Table1:
  EC 1.14.13.219: https://www.genome.jp/entry/1.14.13.219
  EC 1.14.14.41: https://www.genome.jp/entry/1.14.14.41
  EC 1.14.13.234: https://www.genome.jp/entry/1.14.13.234
  EC 1.14.14.38: https://www.genome.jp/entry/1.14.14.38
  EC 1.14.14.39:https://www.genome.jp/entry/1.14.14.39

- The Compound Discoverer™ software (2.1 SP1version, Thermo Scientific) access were used under license from the authors for the current study. Should any extended information be needed in another format they are available from the corresponding author.